Molecular and Subcellular-Scale Modeling of Nucleotide Diffusion in the Cardiac Myofilament Lattice

Peter M. Kekenes-Huskey,[†]* Tao Liao,[‡] Andrew K. Gillette,[§] Johan E. Hake,[¶] Yongjie Zhang,[‡] Anushka P. Michailova,[‖] Andrew D. McCulloch,[‖] and J. Andrew McCammon[††]

[†]Department of Pharmacology, and [§]Department of Mathematics, University of California, San Diego, California; [¶]Simula School of Research and Innovation, Oslo, Norway; [‡]Department of Mechanical Engineering, Carnegie Mellon, Pittsburgh, Pennsylvania; and [‖]Department of Bioengineering, and [††]Howard Hughes Medical Institute, University of California, San Diego, California

Supporting Material

Homogenization

Mesh construction

Meshes were built for both the thin and thick filaments based on (34). For the thin filaments, a multi-level summation of Gaussian kernel functions was applied, for which there are three levels of resolution: atomic, residue, chain and domain. The density distribution of a single atom is represented using the Gaussian kernel function

$$G_{i_A}(\mathbf{x}) = e^{\kappa\left(\|\mathbf{x}-\mathbf{x}_{i_A}\|^2 - r_{i_A}^2\right)}, \tag{S1}$$

where κ is the decay rate, controlling the decay of the Gaussian kernel function. x_{i_A} and r_{i_A} are the center and radius of the i_A^{th} atom, respectively. The Gaussian density of the higher level structures are obtained through the summation of the lower levels:

$$G(\mathbf{x}) = \sum_{i_D}\left(\sum_{i_C}\left(\sum_{i_R}\left(\sum_{i_A} G_{i_A}(\mathbf{x})\right)^{P_R}\right)^{P_C}\right)^{P_D}, \tag{S2}$$

where i_D, i_C, i_R and i_A are the indices of the peptide, residue and atom, respectively. P_R, P_C and P_D are constant coefficients that control the local resolution of the model. By adjusting the parameters, the atomic level feature for the domain TnC and myosin heads are preserved, while the remainder of the thin filament surface is represented at lower resolution. This was accomplished using $P_R = 0.5$ and $P_C = 0.3$ for the low resolution (blurred) region; $P_R = 0.7$ and $P_C = 0.4$ was used for the high-resolution region (TnC and myosin heads). The thick filaments are modeled as simple cylinders. The filaments were assembled into a single Gaussian density map that was inserted into an outer cuboidal boundary. The dual contouring method was then adapted to adaptively generate a tetrahedral mesh from the density map. Quality improvement algorithms such as the face swapping, edge contraction and geometric flow were applied to improve the quality of the tetrahedra.

Validation of the homogenization approach.

To validate our implementation homogenization protocol, we apply the method to 1) a 'layered' problem for which analytical solutions of χ_i are available

(28) and 2) a lattice of parallel cylinders for which numerical estimates of D are provided (26). In 1), we consider a parallel array of impermeable slabs aligned along the x-axis, between which a particle may diffuse (see Fig 6. (28)). We seek χ_i satisfying (2) between the impermeable slabs, thus we created a 2D grid of dimensions 4.2 by 1.3 using Gmsh 2.7 (30). In Figure S3, we show the layered system consisting of a region of free diffusion (triangulated) between two impenetrable layers (gray). We solved (2) on this mesh assuming that the left and right boundaries were permeable (by enforcing periodicity through setting $\chi = 0$), while the top and bottom were impermeable (by enforcing the Neumann condition (2)) . In Figure S3 we plot χ_2 for the model geometry; the Neumann condition defined at the impermeable boundaries adjacent to the slabs (gray) yield a monotonically decreasing χ_2 function along increasing y. The analytical solutions to this problem (see Equations 87a-c in (28)) are given by

$$\chi_1 = \chi_1(x) \tag{S3}$$

$$\chi_2 = -y_2 + \chi_2(x) \tag{S4}$$

$$\chi_3 = \chi_3(x) \tag{S5}$$

We compare the analytical result for χ_2 with our predicted solution in Figure S3 and Figure S4 and find that the solutions are in exact agreement (within an arbitrary constant). Substitution of the $\nabla\chi_i$ into (3) yields the normalized effective diffusion constant, D, as $D = |\Omega_\epsilon|/|\Omega| \equiv \phi$, where ϕ is the accessible volume fraction, for i=1,3 (normal to the layered barriers) and $D = 0$ otherwise.

For 2), we compared the effective diffusivities predicted for cells representing a lattice of parallel cylinders. For the cylinder lattice, we created a unit cell with a circular obstacle of variable radius at its center, similar to Figure 6.14 of (26). In each 1x1x1 Å unit cell we embedded an impermeable cylinder whose radii varied from 0.1 to 0.4 Å, which yielded accessible volume fractions, ϕ, ranging from nearly 1.0 to 0.3. Similar to the layered problem, since the cylinder is invariant along the longitudinal axis, $\chi_z = 0$ and thus $D_L = \phi$, where D_L is the longitudinal component of the normalized effective diffusion constant. Since to our knowledge there are no analytical solutions for the transverse component of the effective diffusivity, D_T, we utilize the upper bound for the parallel cylinder lattice established by Hashin and Shtrikman (see Theory). Our predictions in Figure S5 are in agreement with the analytical value for D_L and the HS scaling relation for D_T. In agreement with intuition, D_T is smaller than D_L for $\phi \leq 1$. Moreover, we observe that the solutions for D_T nearly coincide with the upper

HS bound, as reported in Chapter 6 of (26) and are in agreement with the Maxwell-Garnett estimate reported in Eqn (23) of (41).

Error in homogenization estimates

Several factors could add variability to our estimates of the effective diffusion constants, including the relative arrangement and configuration of the thick and thin filaments, the resolution of the structures, as well as the resolution of the generated meshes. We demonstrated in the Results that the lattice arrangement and myosin head configuration influence D, and these estimates are considerably different from the case in which primitive representations of the filaments are assumed. To understand the variability arising from the mesh generation, we created several meshes at varying resolutions (from 140442 to 240353 vertices), to which we applied the homogenization protocol. We found that the mean D was (0.33, 0.35,0.45) with standard error (0.012,0.003,0.009 for n=4). Therefore, despite a nearly 50% reduction in the number of vertices, the standard error was less than 2%. We expect errors of similar magnitude for the remaining geometries; however, since it was not feasible to rebuild the geometries at several mesh resolutions, we did not provide estimates of the standard error in the reported tables. Nevertheless, based on the error from the most variable component, Dx, the 95% confidence interval is within +- 0.023 of the mean; hence all other means outside this interval are considered significant.

Reaction-Diffusion Model.

Model

The PDE is solved within a half-sarcomere geometry originally proposed in (36) and modified here (Figure S6). We define a region where the thin and thick filaments overlap within the A-band, adjacent to which is the I-band (the thin filaments anchoring region), and within the A-band is the H-zone where the thick filaments are anchored. The longitudinal ($\mathbf{x}$) axis of the sarcomere spans the Z and I zones (1.0 μm), myofibril and mitochondrion compartment are along the radial, or transverse, ($\mathbf{y}$ axis of the cell (1.2 μm), while the $\mathbf{z}$ axis is orthogonal to these axes. We assume the overlap region of the A-band, where ATPase activity occurs, spans x=0.2 to 0.8 and y = 0.0 to 1.0 per Vendelin et al (36). We assume the face at y=1.2 μmborders the inter-membrane space of the mitochondrion; along this boundary, ADP is exchanged with ATP according to the Van Beek model described below. All other boundaries are assumed to be reflective. Simulations were performed

for a 25x25x25 vertex, tetrahedralized mesh, for 1000 ms using time-steps of dt=10 ms and the parameters listed in Table S1. We assumed a piecewise linear continuous Galerkin basis set for the model, which was numerically solved using FEniCS (35). Time-dependence was introduced via the backward Euler approach and Newton's method was used to solve the resulting nonlinear problem.

For each time-step the mitochondrial ODE model provided an updated value of the nucleotide fluxes; the ODE model's estimates for $J_{hydrolysis}$ and J_{CK} were applied as source conditions in the PDE, whereas J_{diff} was applied as a boundary conditions. The ODE model was similarly updated with [ATP] and [ADP] predicted by the PDE model. The Van Beek ODE model was acquired from the CellML repository (http://www.cellML.org), pythonized via gotran (available at https://bitbucket.org/johanhake/gotran), and solved using the scipy function 'odeint' at 10,000 time points between the PDE time-intervals (dt=10ms). In Figure S7a we report the input time-dependent myosin ATPase rate ; all other states and fluxes are obtained by solving the ODE at each time step. The combined PDE and ODE model was analyzed for a 1000 ms time interval, following a 5 s equilibration period for the ODE model. To examine ADP gradients developed in absence of the CK pathway, we reduced the forward and backward rates of the CK equation by 98% as per (37). Details of our validation of the implementation are given in the Supporting Material. The code will be released at https://bitbucket.org/huskeypm/sarcomere.

Table S1: **Parameters**. *With exception to the listed quantities, all parameters for the Van Beek model are described in (37)*

Parameter	Value	Description
r_{ATP}	0.66	radius of ATP [nm]
D^{ϵ}_{ATP}	145	Bulk diffusion constant of ATP [μm^2/s] (36)
D^{ϵ}_{ADP}	145	Bulk diffusion constant of ADP [μm^2/s] (36)
$D_{reduced,i}$	0.1 $\cdot D_{bulk,i}$	Reduced diffusion constant of component i in muscle (Est)
$d_{card,MA}$	18.3	Cardiac myosin/actin distance [nm] (Est. from (14))
$d_{skel,MA}$	16.5	Skeletal myosin/actin distance [nm] (9)

Validation of Metabolism model

We validated our implementation in Figure S7, which shows that the average cytosolic nucleotide concentrations under two ATPase hydrolysis frequencies (135 and 220 BPM) are in sync with predictions given in Fig 2 of (37). In Figure 7(b), we show that ADP oscillations upon reduction of CK activity (VCK=0.02) in our model is in good agreement with Fig. 10 of (37). Because we did not explicitly rescale the amplitude of JATP for the VCK=0.02 case, the minimum ADP— concentration in our simulations (0.01 mM) are lower than the estimates in their figure (0.04). JCK/JATP and the diffusion fluxes estimated by the cellML code were passed to the finite element model as source and boundary conditions, respectively (Figure S9 for predicted values). Comparison of estimates from our finite element model Figure S8 with the cellML [ADP] predictions for vCK=1.0 and 0.02 demonstrate equivalent results.

Supplemental figures

Figure S1

Model lattice geometries a) Primitive unit cell for myofibril lattice. Thick (large diameter) and thin (small diameter) filament arrangement follows typical interfilament spacing in cardiac myofibrils. b) Unit cell akin to Shorten's geometry in Fig. 5 (9).

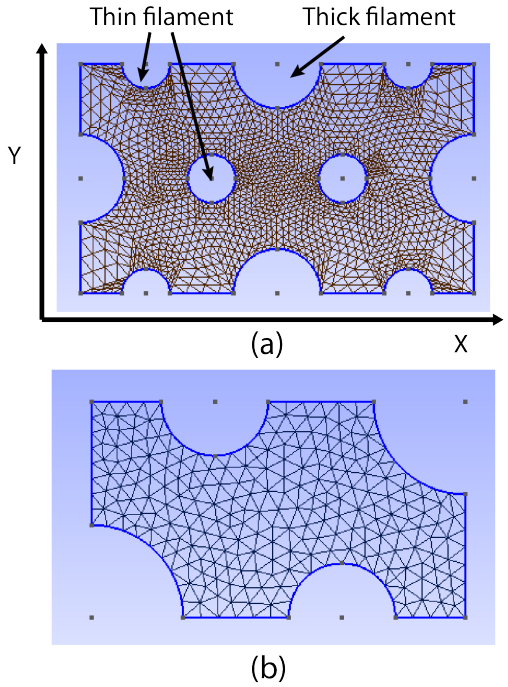

Figure S1:

Figure S2

Solutions of the homogenized diffusion equation χ_x satisfying Equation (2) based on the primitive myofibril unit cell (Figure S1) for diffusing particle diameters of 0 (a) and 6 nm (b). The thick filaments are represented by the large half-cylinders on the unit cell edges, while the thin filaments are interspersed along the cell edges and interior. Diffusional hindrance transverse to the myofibril lattice are evidenced by non-zero (red,blue) values of χ_x.

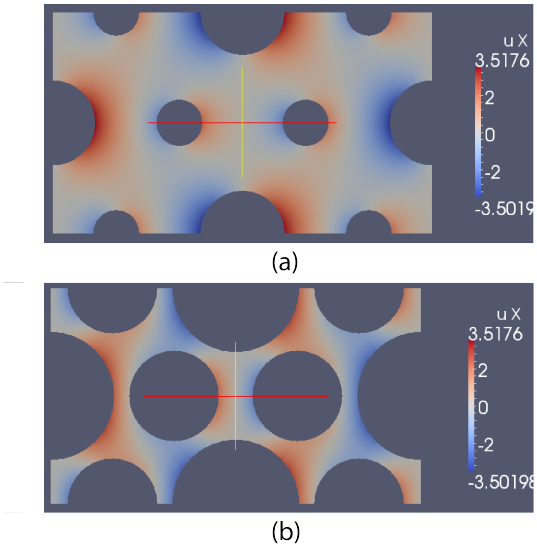

Figure S2:

Figure S3

Predicted χ_2 **solution for layered medium** . Predicted χ_2 field (aligned with the y-axis) for a layered slab. Substrate may freely diffuse along the x direction (left/right) but is impeded by the gray slabs along the y-direction.

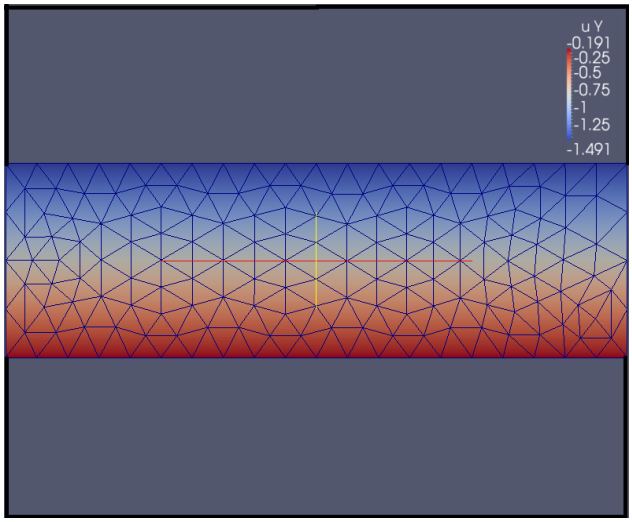

Figure S3:

Figure S4

Predicted χ_2 values for layered medium versus analytical solution Values of χ_2 extracted at x=0 from solution in Figure S4.

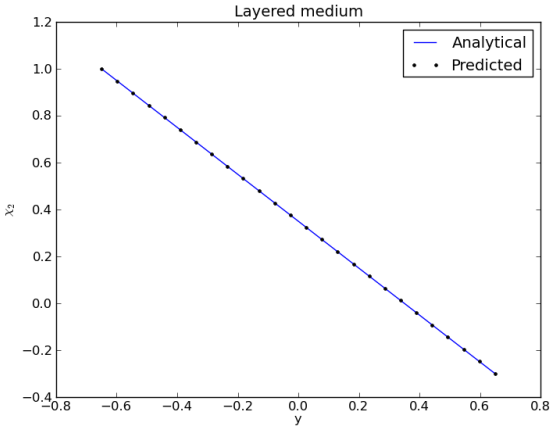

Figure S4:

Figure S5

Comparison of predicted effective diffusion constants for a lattice of parallel cylinders. Triangle and circle symbols correspond to our predictions D parallel, D_L, and transverse, D_T, to cylinders of increasing free volume, ϕ (and decreasing radius). The dashed line represents the analytical solution for D_L and upper bounds for D_T (26).

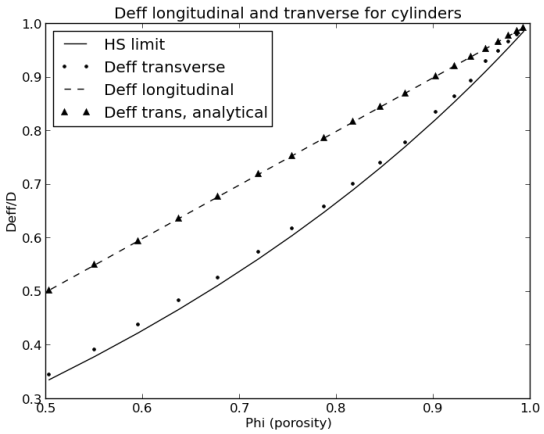

Figure S5:

Figure S6

Half-sarcomere model Half-sarcomere geometry based on Vendelin et al. (36). Region of thin and thick filament overlap designated as the A-band. Adjacent to the A-band are the I-band, which contains the Z-line, and at the A-band center is the H-zone, which contains the M-line. The longitudinal axis (x) of the sarcomere is 1.0 μm in length; the circumferential axis of the cell (y) is 1.2 μm in width. The **z** axis is aligned with the transverse direction of the cell. The overlap region of the A-band, where ATPase activity occurs, spans x=0.2 to 0.8 and y = 0.0 to 1.0 per Vendelin et al. (36). The face at y=1.2 μmborders the intermembrane space of the mitochondrium; along which ADP is exchanged with ATP via the diffusional fluxes $J_{diff,ATP}$ and $J_{diff,ADP}$. All other boundaries are assumed to be reflective.

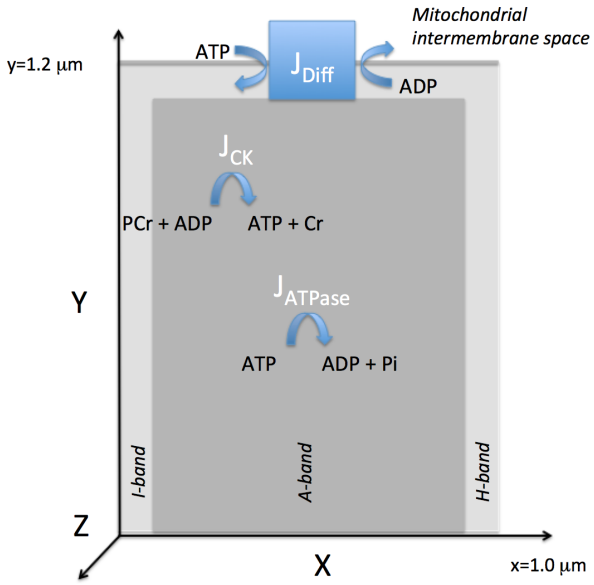

Figure S6:

Figure S7

Time course of the ATP hydrolysis flux a) JATP predicted by our implementation of Van Beek's cellML metabolism model (37) at 135 beats per minute (0-2 s) and 220 BPM (2-10 s) and applied to our finite element model. b) Validation of our implementation of the Van Beek code, in which the time course of ADP is presented under varying levels of creatine kinase activity (vCK=1.0 and 0.02, compare with Figure 10 of (37)) .

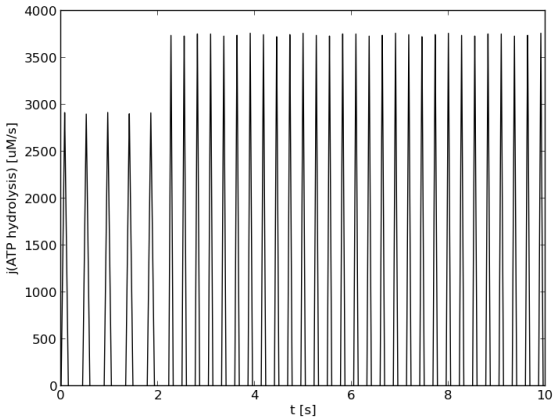
4000
3500
3000
2500
2000
1500
1000
500
0
j(ATP hydrolysis) [uM/s]
0
2
4
6
8
10
t [s]

(a)

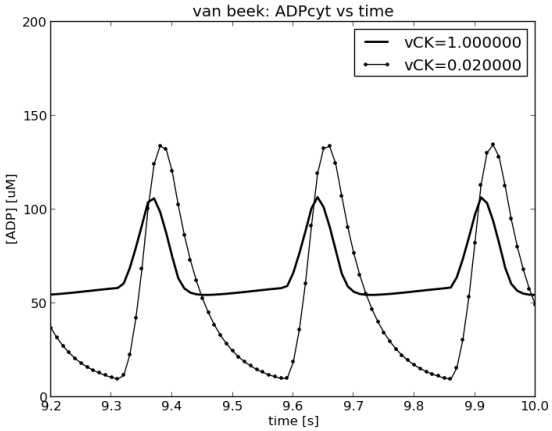
van beek: ADPcyt vs time
vCK=1.000000
vCK=0.020000
200
150
100
50
0
[ADP] [uM]
9.2
9.3
9.4
9.5
9.6
9.7
9.8
9.9
10.0
time [s]

(b)

Figure S7:

Figure S8

Predicted average ATP and ADP concentrations. Nucleotide concentrations predicted by the half-sarcomere finite element model over a 1 second interval using the anisotropic (Deff/D=[x,y,z], symbols) diffusion constant computed from the thin filament representation with three cross bridges, as well as the unhindered, isotropic diffusion constant (Deff/D=1.0, lines).

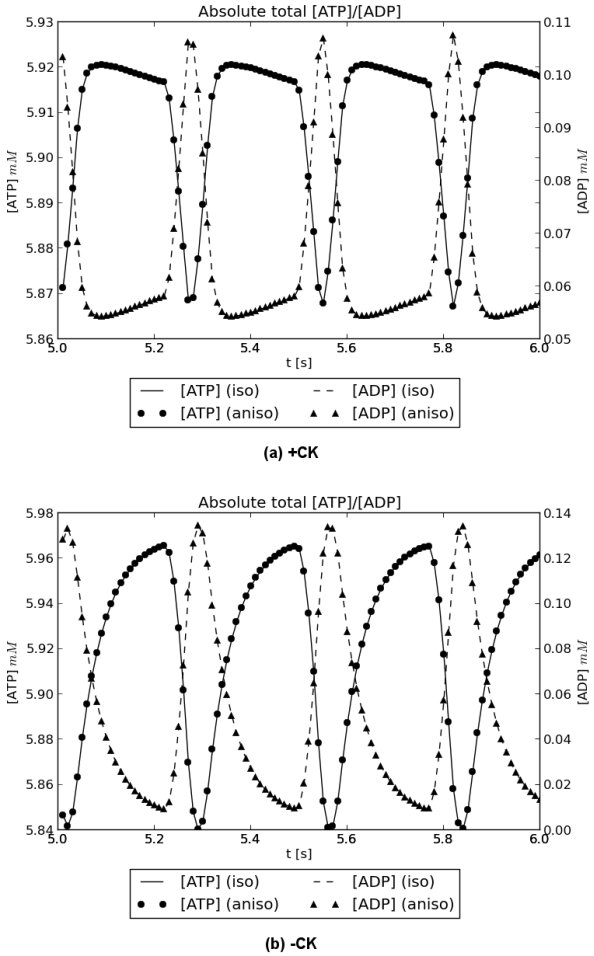

Figure S8:

Figure S9

Predicted average ATP hydrolysis and ATP diffusional fluxes from the PDE simulation. ATP fluxes originating from ATP hydrolysis (solid), the cytosolic creatine kinase reaction (dot dash) and the nucleotide exchange with the mitochondrion (dashed) are presented a) with CK and b) without CK activity.

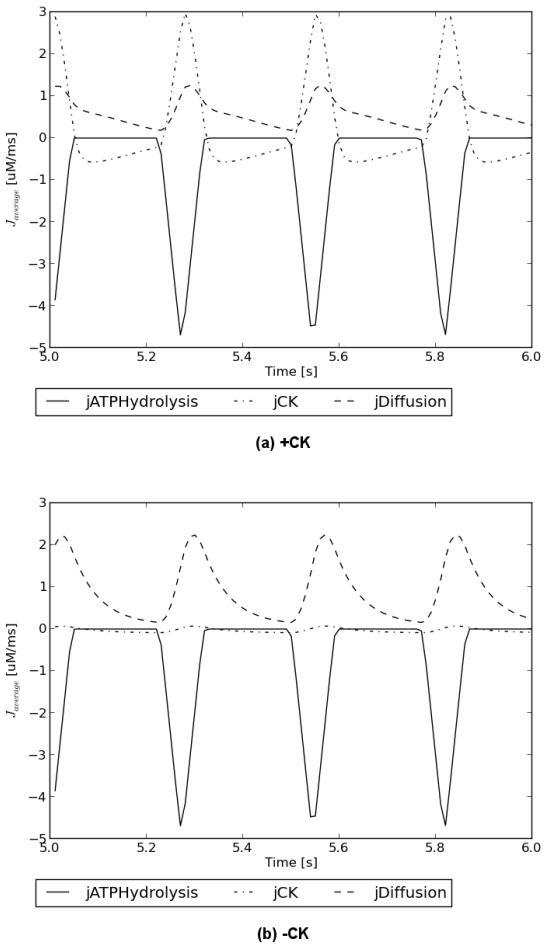

Figure S9:

Figure S10

Two-dimensional ADP concentrations. Reported at 5.3 s (corresponding to peak myosin ATPase activity) in the presence of CK (a,b) and in its absence (c,d), for the isotropic (a,c) and anisotropic (b,d) diffusion coefficients.

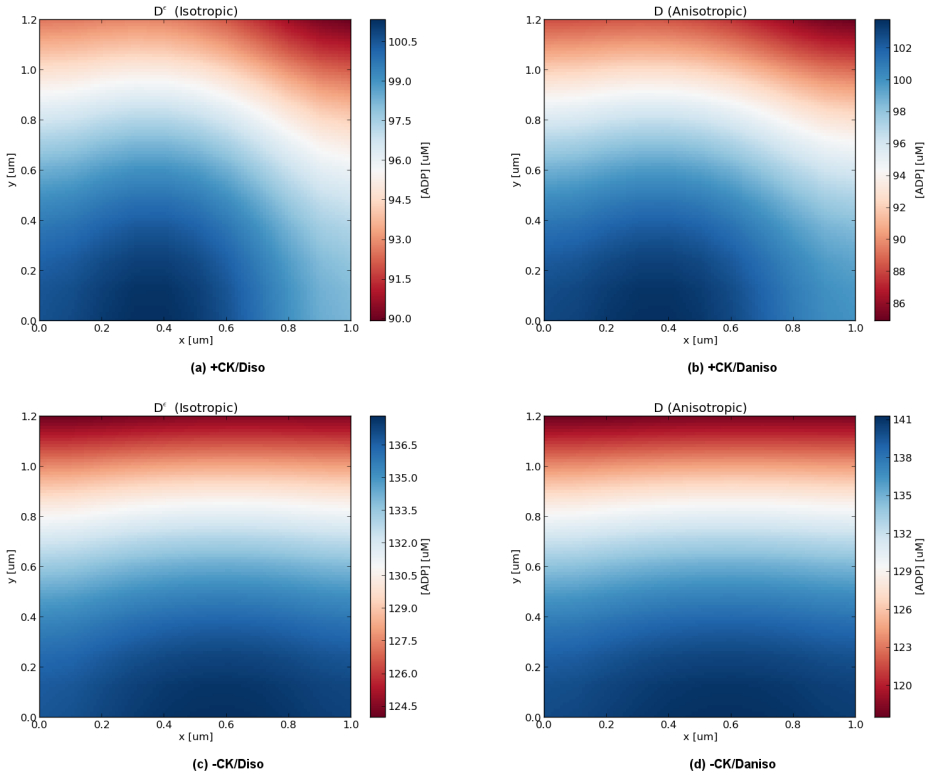

Figure S10:

Figure S11

Same as Figure S10, but with D reduced by ten-fold.

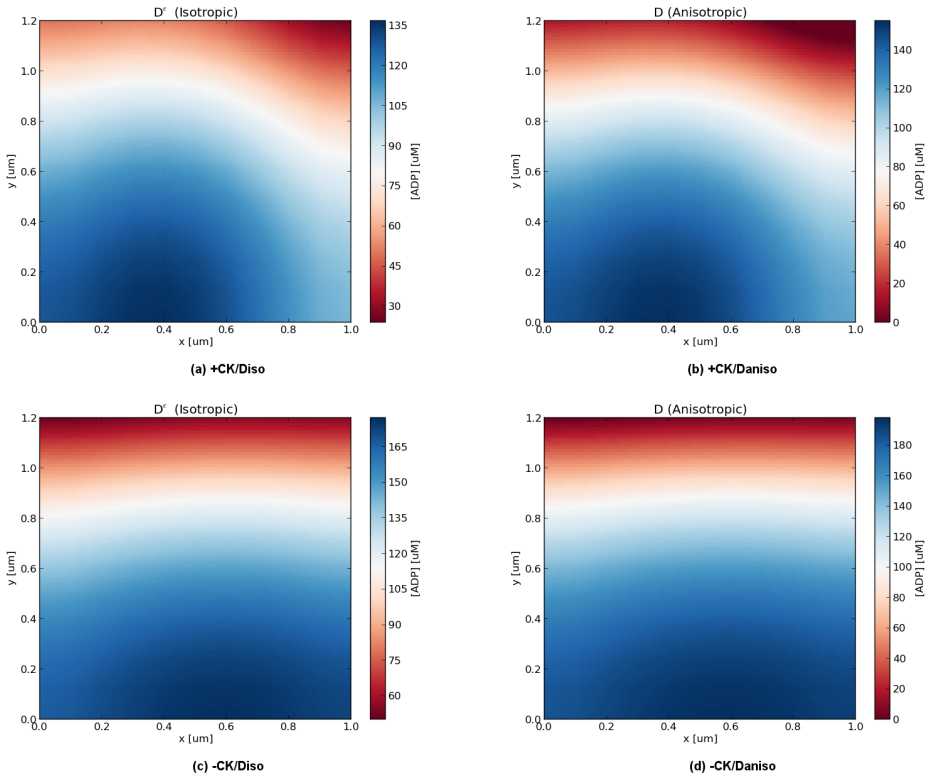
D^r (Isotropic)
D (Anisotropic)
y [um]
x [um]
[ADP] [uM]
(a) +CK/Diso
(b) +CK/Daniso
(c) -CK/Diso
(d) -CK/Daniso

Figure S11: